Electronic Supplementary Material (ESI) for Energy & Environmental Science.
This journal is © The Royal Society of Chemistry 2014

Electronic Supplementary Information (ESI)

Band engineering of high performance p-type FeNbSb based half-Heusler thermoelectric materials for figure of merit zT>1

*Chenguang Fu[a], Tiejun Zhu[*a,b], Yintu Liu[a], Hanhui Xie[a] and Xinbing Zhao[a,b]*

[a] State Key Laboratory of Silicon Materials, Department of Materials Science and Engineering, Zhejiang University, Hangzhou 310027, China

[b] Key Laboratory of Advanced Materials and Applications for Batteries of Zhejiang Province, Zhejiang University, Hangzhou 310027, China

*E-mail: zhutj@zju.edu.cn

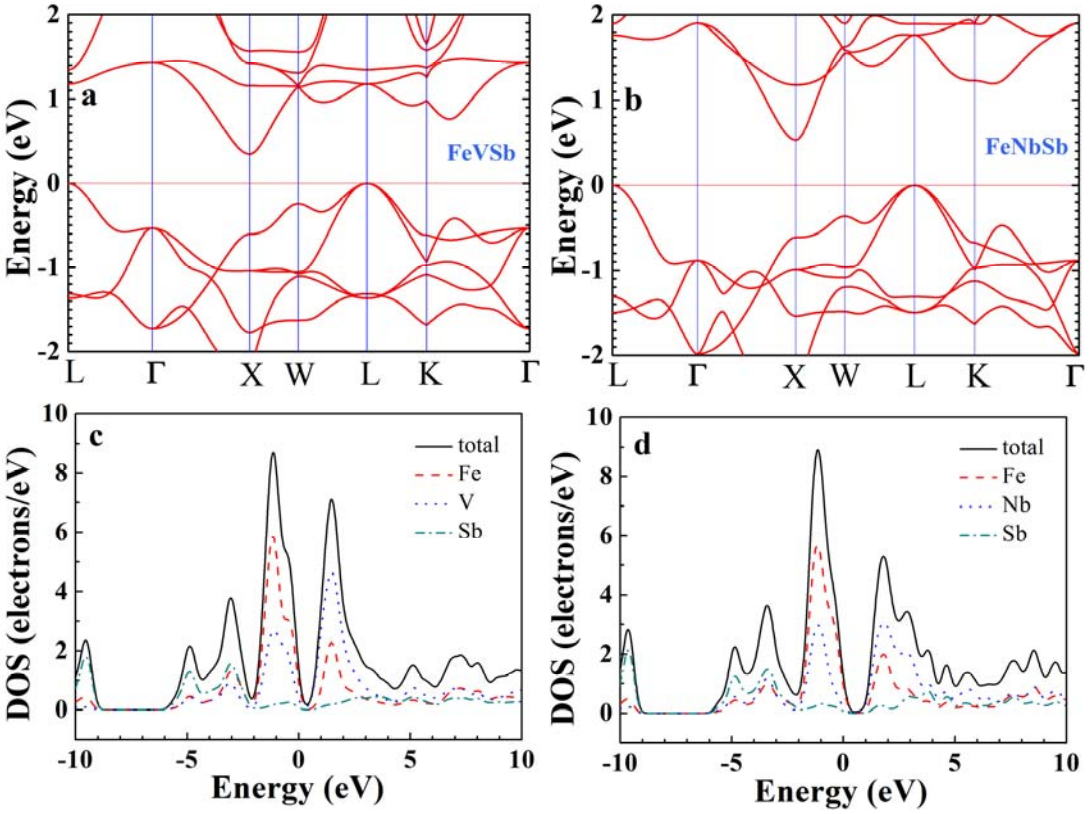

Fig. S1. Band structures and total and partial density of states (DOS) for FeVSb (a, c) and FeNbSb (b, d).

Table S1. The calculated effective masses using the curvature of the valence bands. The values related to the transport properties are given with the unit of m^*/m_e. Three values are calculated along different directions. Table S1 shows the calculated effective masses of FeVSb along different directions are all larger than that of FeNbSb, indicating increasing Nb content in $Fe(V_{1-y}Nb_y)_{1-x}Ti_xSb$ may lead to lower band effective mass.

Compound	band	m^*/m_e	m^*/m_e	m^*/m_e	m_b^*/m_e
		LW	LK	$L\Gamma$	
FeVSb	VBM-light	0.6	0.6	2.8	1.0
	VBM-heavy	0.9	0.9	2.8	1.3
FeNbSb	VBM-light	0.5	0.5	2.1	0.8
	VBM-heavy	0.7	0.7	2.1	1.0

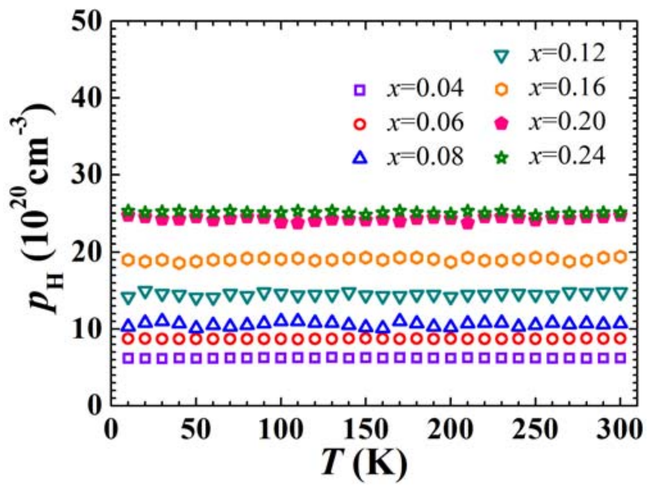

Fig. S2. Temperature dependence of carrier concentration for $FeNb_{1-x}Ti_xSb$ samples.

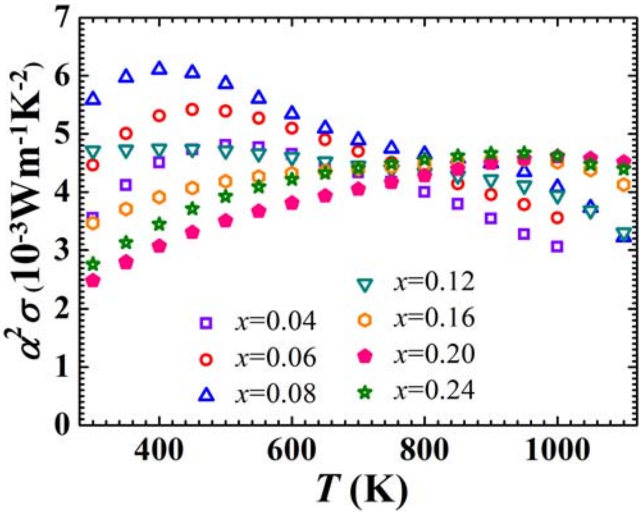

Fig. S3. Temperature dependence of power factor for $FeNb_{1-x}Ti_xSb$ samples.

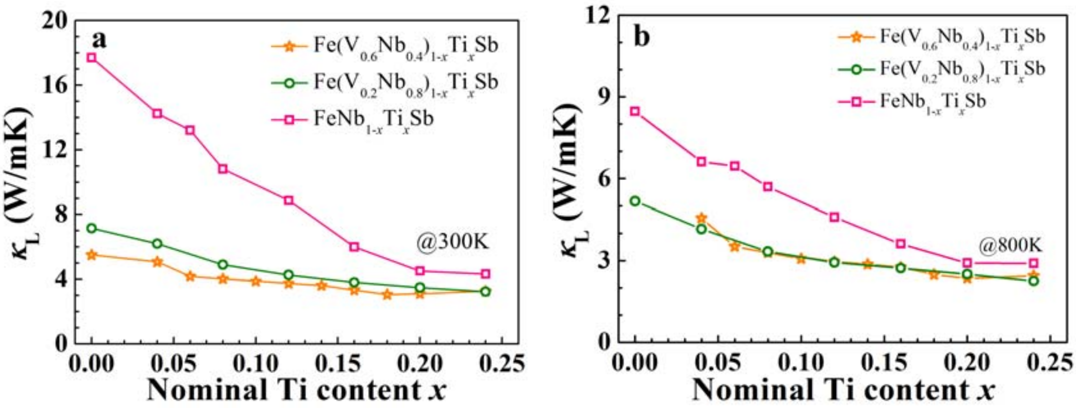

Fig. S4. Lattice thermal conductivity of $Fe(V_{1-y}Nb_y)_{1-x}Ti_xSb$ samples versus nominal Ti content x at 300K (a) and 800K (b).

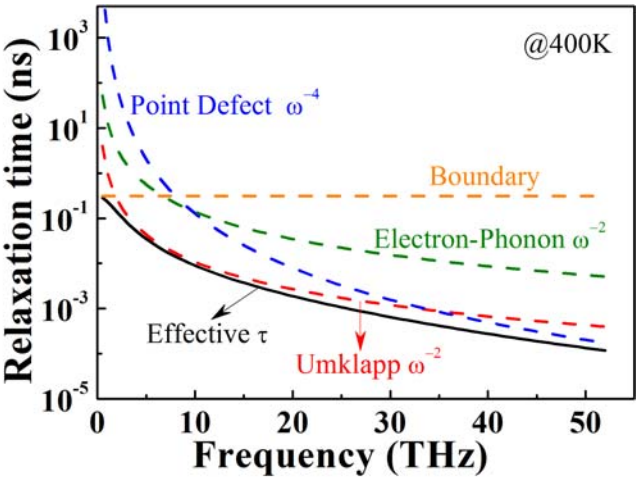

Fig. S5. Calculated phonon relaxation time τ versus frequency ω at 400K for $FeNb_{0.8}Ti_{0.2}Sb$ sample.

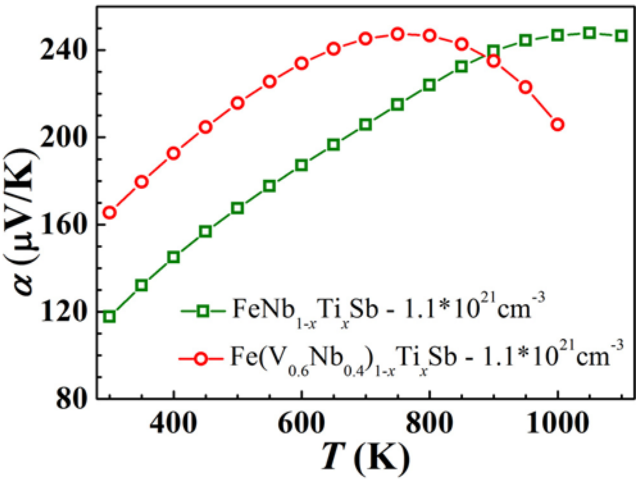

Fig. S6. Seebeck coefficient α versus temperature for $FeNb_{1-x}Ti_xSb$ and $Fe(V_{0.6}Nb_{0.4})_{1-x}Ti_xSb$ with the same carrier concentration. The peak value of α indicates the intrinsic excitation temperature of $FeNb_{1-x}Ti_xSb$ is higher than that of $Fe(V_{0.6}Nb_{0.4})_{1-x}Ti_xSb$.

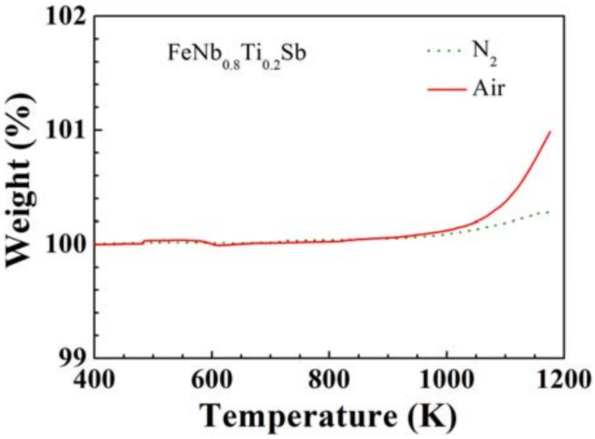

Fig. S7. Thermogravimetric analysis for $FeNb_{0.8}Ti_{0.2}Sb$ under air and N_2 atmosphere respectively. When heating in the air atmosphere, there is no weight loss or gain for $FeNb_{0.8}Ti_{0.2}Sb$ until 1000K, indicating good high temperature stability. Above 1000K, slight weight gain which may result from the surface oxidation. The sample displays excellent stability when heating in the N_2 atmosphere.

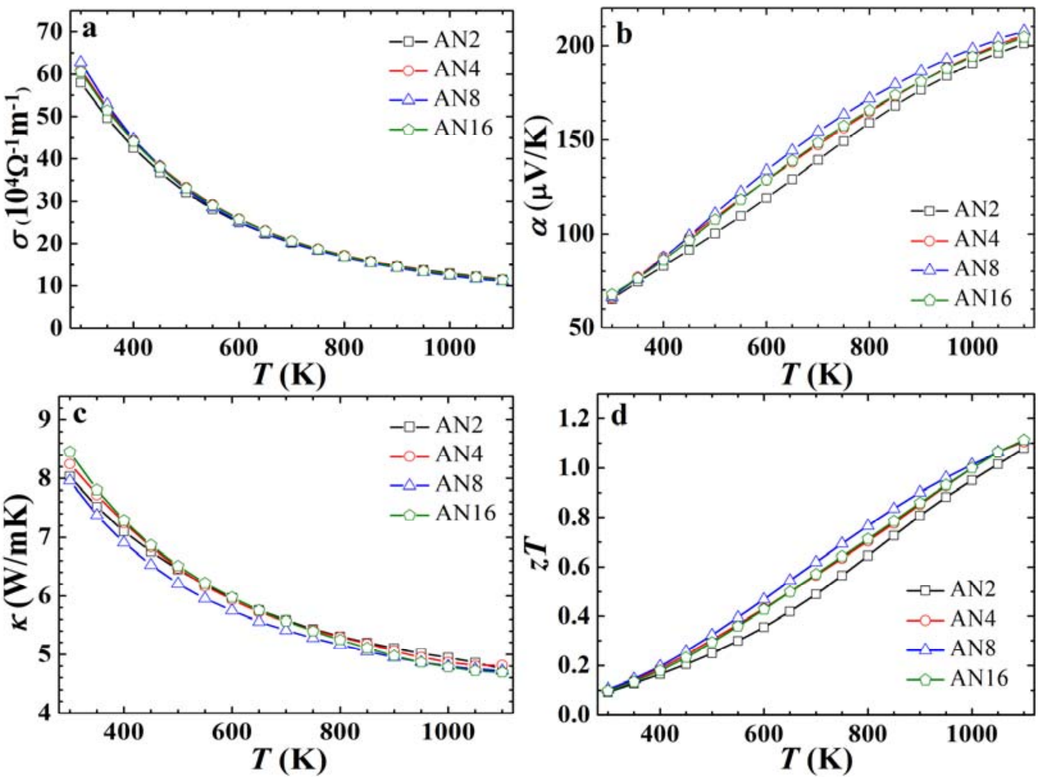

Fig. S8. Reproducibility and TE properties versus temperature for 4 independent samples of $FeNb_{0.8}Ti_{0.2}Sb$ annealed (AN) for 2, 4, 8, and 16 days respectively. (a) Electrical conductivity, (b) Seebeck coefficient, (c) Thermal conductivity, and (d) *zT* value.

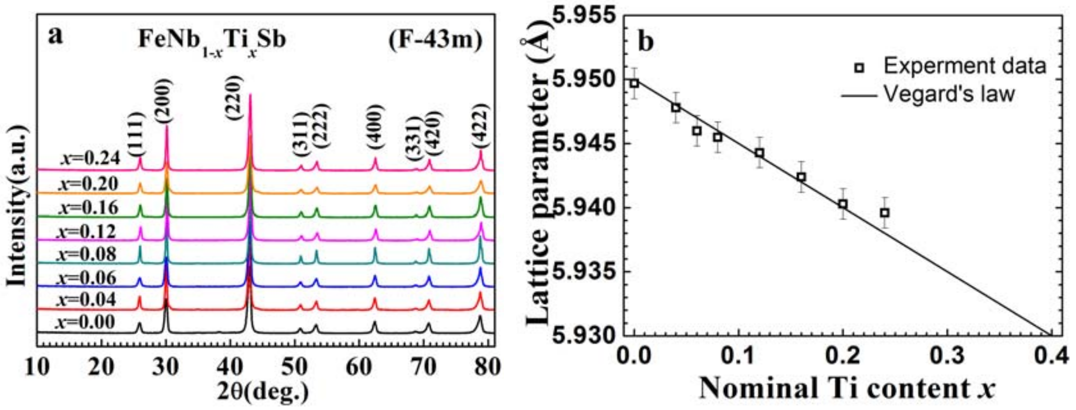

Fig. S9. (a) XRD patterns of $FeNb_{1-x}Ti_xSb$ (x = 0~0.24) samples. (b) Lattice parameters of $FeNb_{1-x}Ti_xSb$ follow the Vegard's law up to x=0.2 (the straight line).

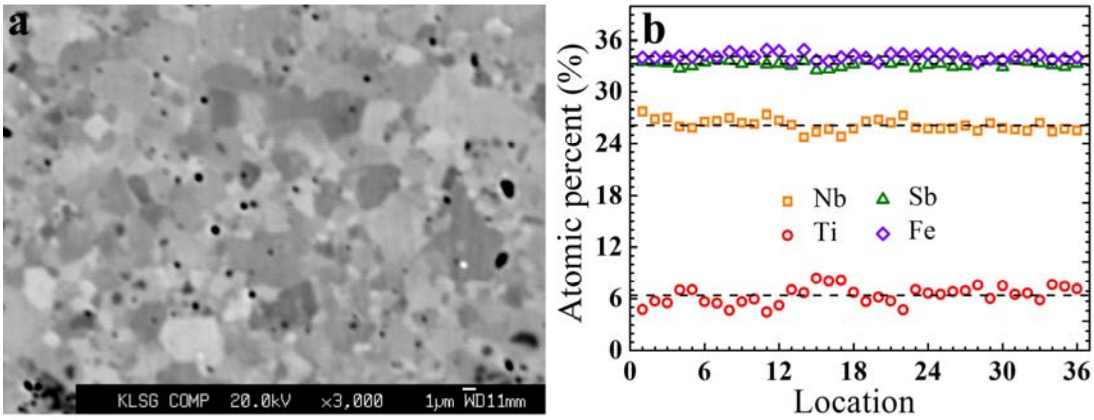

Fig. S10. (a) Typical back scattering electron image for $FeNb_{1-x}Ti_xSb$ samples. Black holes are pores and grain contrast should result from the different grain orientations. (b) Percent atomic composition of $FeNb_{0.8}Ti_{0.2}Sb$ at 36 randomly selected locations from 4 independent samples, suggesting the samples are macroscopically homogeneous. The dash lines point out the average values.

Table S2. The nominal composition, EPMA composition, the relative density, and lattice parameter for $FeNb_{1-x}Ti_xSb$ (x = 0.04 ~ 0.24) samples.

Nominal composition	EPMA composition	Relative density (%)	Lattice parameter (Å)
FeNbSb	$Fe_{1.02}Nb_{0.98}Sb$	95.1	5.949(7)
$FeNb_{0.96}Ti_{0.04}Sb$	$Fe_{1.02}Nb_{0.94}Ti_{0.04}Sb$	96.2	5.947(8)
$FeNb_{0.94}Ti_{0.06}Sb$	$Fe_{1.02}Nb_{0.92}Ti_{0.05}Sb_{1.01}$	96.9	5.946(0)
$FeNb_{0.92}Ti_{0.08}Sb$	$Fe_{1.02}Nb_{0.90}Ti_{0.08}Sb$	95.5	5.945(5)
$FeNb_{0.88}Ti_{0.12}Sb$	$Fe_{1.02}Nb_{0.86}Ti_{0.11}Sb_{1.01}$	96.7	5.944(3)
$FeNb_{0.84}Ti_{0.16}Sb$	$Fe_{1.02}Nb_{0.82}Ti_{0.16}Sb$	95.7	5.942(4)
$FeNb_{0.80}Ti_{0.20}Sb$	$Fe_{1.02}Nb_{0.8}Ti_{0.18}Sb$	95.3	5.940(3)
$FeNb_{0.76}Ti_{0.24}Sb$	$Fe_{1.02}Nb_{0.76}Ti_{0.22}Sb$	97.1	5.939(6)

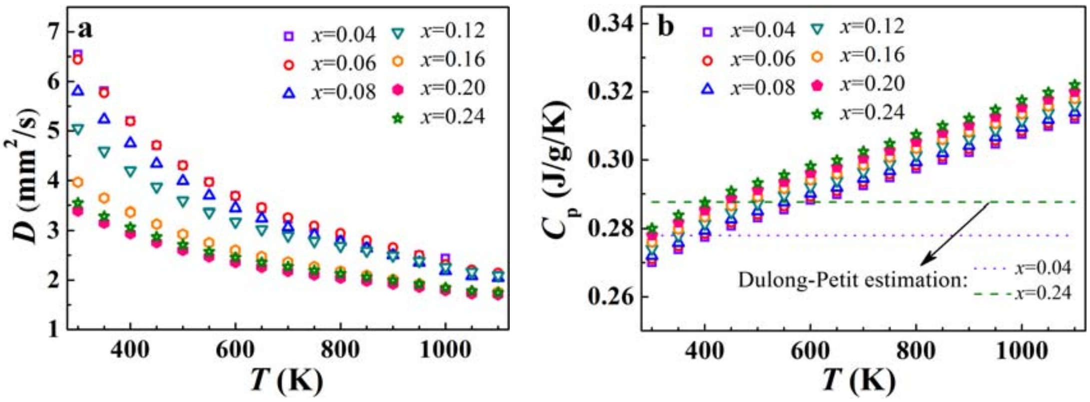

Fig. S11. Temperature dependence of thermal diffusivity (a) and specific heat (b) for $FeNb_{1-x}Ti_xSb$ (x = 0~0.24) samples. The dash lines in (b) represent the Dulong-Petit estimation.

Electronic structure calculation

Electronic structure calculations of FeVSb and FeNbSb were performed with the Perdew-Burke-Ernzerhof[1] generalized gradient approximation and projected augmented wave method,[2] as implemented in *Vienna AB initio Simulation Package*.[3] A plane-wave cutoff energy of 400 eV and an energy convergence criterion of 10^{-4} eV for self-consistency are adopted throughout the calculations. For static calculation, a 15 × 15 × 15 Monkhorst–Pack k-point sampling is used for the primitive unit cell with 3 atoms.[4] The accuracy of the band-structure calculations using VASP is checked by comparing with those obtained from Korrings-Kohn-Rostoker calculations with the coherent potential approximation.[5] We find that both results agree well with each other.

Phonon relaxation time calculation

Callaway had proposed a phenomenological model about the lattice thermal conductivity, which is expressed as:[6]

$$\kappa_L = \frac{k_B}{2\pi^2 v}\left(\frac{k_B T}{\hbar}\right)^3 \int_0^{\theta_D/T} \frac{x^4 e^x}{\tau^{-1}(e^x-1)^2}\,dx\,, \tag{1}$$

where $x = \hbar\omega / k_B T$ is the reduced phonon frequency, k_B the Boltzmann constant, $\hbar$ the reduced Planck constant, θ_D the Debye temperature, v the sound velocity, and τ the effective relaxation time, which can be written as

$$\tau^{-1} = A\omega^4 + B\omega^2 T\exp(-\theta_D/3T) + C\omega^2 + \frac{v}{d}\,, \tag{2}$$

where *d* is the grain size and *v/d* represents boundary scattering, and *A*, *B*, *C* are the prefactors for point defect (PD) scattering, phonon-phonon Umklapp (U) scattering, and electron-phonon (EP) scattering, respectively.

For the polycrystalline pure FeNbSb, the dominated phonon scattering mechanism should be the phonon-phonon U scattering and boundary scattering. Therefore, through fitting the κ_L of polycrystalline FeNbSb, we can obtain the prefactor *B* of U scattering. Scattering by point defects arises from both mass and strain differences within the lattice. In the simple case of alloying, $\tau_{PD}^{-1} = \frac{V\omega^4}{4\pi v^3}(\Gamma_M + \Gamma_S)$, where Γ_M and Γ_S are the disorder scattering parameters due to mass and strain field fluctuations, respectively. The detailed calculation of point defects scattering can be found elsewhere.[7,8] For $FeNb_{0.8}Ti_{0.2}Sb$, the existing phonon scattering sources should contain the U process, boundary, point defects and electron-phonon interaction. The boundary scattering and point defects scattering can be calculated independently, while U scattering relaxation time can be obtained from fitting the polycrystalline FeNbSb. Therefore, through fitting the κ_L of $FeNb_{0.8}Ti_{0.2}Sb$, we can obtain the prefactor of EP scattering. And then we can calculate the frequency dependence of phonon relaxation time for $FeNb_{0.8}Ti_{0.2}Sb$ sample.

References

1 J. P. Perdew, K. Burke and M. Ernzerhof, *Phys. Rev. Lett.*, 1996, **77**, 3865.

2 P. E. Blochl, *Phys. Rev. B*, 1994, **50**, 17953.

3 G. Kresse and J. Furthmuller, *Phys. Rev. B*, 1996, **54**, 11169.

4 H. J. Monkhorst and J. D. Pack, *Phys. Rev. B*, 1976, **13**, 5188.

5 L. Jodin, J. Tobola, P. Pecheur, H. Scherrer and S. Kaprzyk, *Phys. Rev. B,* 2004, **70**, 184207.

6 J. Callaway, *Phys. Rev.*, 1959, **113**, 1046.

7 C. G. Fu, H. H. Xie, T. J. Zhu, J. Xie and X. B. Zhao, *J. Appl. Phys.*, 2012, **112**, 124915.

8 J. Yang, G. P. Meisner and L. Chen, *Appl. Phys. Lett.*, 2004, **85**, 1140.